Environmental Science & Technology

pubs.acs.org/est

Article

Unexpectedly High Indoor HONO Concentrations Associated with Photochemical NO_2 Transformation on Glass Windows

Jiangping Liu, Huifan Deng, Pascale S. J. Lakey, Haoyu Jiang, Majda Mekic, Xinming Wang, Manabu Shiraiwa,* and Sasho Gligorovski*

Cite This: *Environ. Sci. Technol.* 2020, 54, 15680−15688

Read Online

ACCESS | Metrics & More | Article Recommendations | Supporting Information

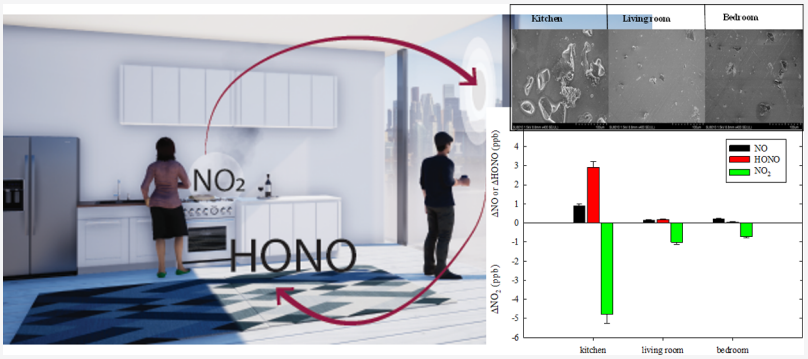

ABSTRACT: Nitrous acid (HONO) is an important gaseous pollutant contributing to indoor air pollution because it causes adverse health effects and is the main source of hydroxyl radicals (OH). Here, we present direct measurements of HONO produced through light-induced heterogeneous reactions of NO_2 with grime adsorbed on glass window. The uptake coefficients of NO_2 [$\gamma(NO_2)$] on the glass plates from the kitchen increased markedly from $(2.3 \pm 0.1) \times 10^{-6}$ at 0% RH to $(4.1 \pm 0.5) \times 10^{-6}$ at 90% RH. We report a significant quantity of daytime HONO produced in the kitchen, compared to the living room and bedroom. Kinetic modeling suggests that phase state and bulk diffusivity play important roles in the NO_2 uptake; the best fit to the measured uptake coefficients is obtained with fixed diffusion coefficients. Photon scattering may be occurring at the surface of the films, leading to enhanced photon-excitation rates of polycyclic aromatic hydrocarbons. By taking these effects into account, the results from this study indicate that the HONO yields obtained in this study can explain the missing HONO in the photochemical models describing the indoor air chemistry.

INTRODUCTION

Understanding the formation of nitrous acid (HONO) is of particular interest as HONO causes adverse health effects[1,2] and represents a major precursor of hydroxyl radicals (OH) in sunlit indoor air.[3−5] However, our understanding of HONO formation processes in the indoor atmosphere lags substantially behind that for outdoor processes.[6]

Gaseous HONO can be generated in substantial mixing ratios, ranging from 20 to 90 ppb, through combustion processes (e.g., cooking, gas stoves, gas-fired kitchen range, space heaters, and lighting candles or incenses).[4,5,7−9] A pioneering scientific investigation[10] suggested that in the absence of UV light and combustion processes, the heterogeneous hydrolysis of nitrogen dioxide (NO_2) on indoor surfaces can be a major HONO source. This observation was confirmed in a more recent study by Finlayson-Pitts and her co-workers,[11] showing that the heterogeneous HONO production proceeds faster at higher levels of NO_2 and relative humidity (RH %).

HONO formation through heterogeneous conversion from NO_2 is enhanced significantly during the day in sunlit regions of the indoor environment.[12−14] The mixing ratios of NO_2 in indoor air vary between 15 ppb in the absence of human activities and 200 ppb in the presence of combustion sources.[3,5,15,16] NO_2 easily adsorbs on various impermeable indoor surfaces and reacts with adsorbed organic compounds.[11] The organic films on various indoor surfaces are reported to be typically 4−30 nm thick, which initially build up at a faster formation rate and then slowly grow over time.[17] The sources of these organic compounds are diverse including exchange with outdoor air, building materials, furniture, insect

Received: August 20, 2020
Revised: October 5, 2020
Accepted: November 12, 2020
Published: November 24, 2020

repellants, personal care products, cleaning, and cooking. Cleaning products release terpene compounds in indoor air such as D-limonene and α-terpinene, with average concentrations between 5 and 15 ppb.[18] Simulations on a molecular level have shown that volatile compounds such as D-limonene adsorb on glass surfaces within microseconds[19] and react with indoor oxidants such as ozone (O_3)[20] and NO_2.[12] Cooking activities represent a source of fatty acids and polycyclic aromatic hydrocarbons (PAHs).[21,22] These compounds can be easily adsorbed on impervious indoor surfaces and react with indoor air oxidants including NO_2 and O_3. The products of such reactions remain on the surface or desorb to the gas phase. Glass windows are directly irradiated by sunlight during certain periods of the day depending on the solar zenith angle and the orientation of the building.[23] At present, known sources of HONO are poorly understood and do not account for observed levels in the indoor atmosphere.

To our knowledge, this is the first investigation on the heterogeneous reaction of NO_2 with authentic grime adsorbed on indoor glass surfaces in the dark and in the presence of simulated sunlight irradiation. The uptake coefficients of NO_2 on glass window surfaces collected from the kitchen, living room, and bedroom were compared in the dark and under light irradiation at different RH. Here, we show that much higher quantities of HONO are formed upon light-induced heterogeneous conversion of NO_2 on a glass surface in the kitchen compared to glass surfaces in the bedroom and living room. The kinetic multi-layer model of aerosol surface and bulk chemistry (KM-SUB)[24] was applied to investigate NO_2 uptake coefficients and HONO surface fluxes for the indoor surface films as a function of RH.

MATERIALS AND METHODS

Grime on Indoor Glass Surface. The grime was collected by placing several rectangular borosilicate glass plates (50 cm × 1.5 cm) in the bedroom, living room, and kitchen of an apartment located in downtown Guangzhou, China (Text S2). The glass plates were mounted onto a frame (150 cm × 50 cm) and positioned horizontally near the windows in the rooms. Cooking activities were undertaken almost every day during this period. After a period of 4 weeks, the glass plates were collected and carefully taken to the laboratory for further investigations by gas chromatography/mass spectrometry (GC−MS) and ultra-high-resolution scanning electron microscopy (UHR-SEM) and for assessing the NO_2 heterogeneous reactions in the flow tube reactor.

Flow Tube Reactor. The heterogeneous reactions of gaseous NO_2 with the glass plates were performed in a flow tube reactor. The flow tube reactor is designed to operate at ambient pressure under gas-phase laminar flow conditions. The flow tube reactor was applied in our previous studies to evaluate the uptake coefficients of NO_2 on various indoor surfaces (paint, lacquer, and cleaning detergents) and outdoor urban grime.[12−14,25]

Briefly, the flow reactor is made out of a cylindrical glass tube (length = 50 cm, inner diameter = 2.6 cm) inserted into a double-wall glass tube which is connected to a thermostatic bath (Lauda RC6 refrigerated bath with RCS thermostat, temperature accuracy = ±0.02 K at 263 K), allowing the experiments to be performed at a constant temperature of 296 K. A movable glass injector with a fritted end was used to introduce the NO_2 into the flow tube reactor.

Only one side of the glass plates is covered with grime. Glass plates are inserted in the flow tube with the side covered with grime upward oriented toward the lamp to ensure complete irradiation of the surface. The dimensions and flows in the flow tube were chosen to ensure laminar conditions. A sheath flow of N_2 was used which avoids retro-diffusion of NO_2 in the reactor. The length of the glass plate is identical with the dimension of the flow reactor which allows to be perfectly fitted into the reactor without perturbation of the laminar flow.

These conditions ensure that only the upper sides of the plates which are covered with grime are exposed to NO_2 and to light irradiation.

A certified mixture of NO_2 (10 ppm) in nitrogen (N_2) (99.999% MESSER) was connected to a mixing loop fed by N_2 (99.999% MESSER) to allow dilution. A NO_2 flow of 10 mL min^{-1} (0−100 mL min^{-1} HORIBA METRON mass flow controller; accuracy, ±1%) is incorporated into the 200 mL min^{-1} synthetic air flow (0−1000 mL min^{-1} HORIBA METRON mass flow controller; accuracy, ±1%).

A sheath flow (N_2) of 1000 mL min^{-1} (0−1000 mL min^{-1} HORIBA METRON mass flow controller; accuracy, ±1%) was fed to a bubbler before its introduction in the reactor to obtain the required mixing ratios of NO_2 typical for the indoor environment. RH was adjusted by splitting this sheath flow in two fluxes, one of dry air flow and the other humidified by bubbling through ultrapure water (Sartorius, 18 MΩ, H2O-MM-UV-T, Germany). A mixing of these two flows at different ratios created a carrier gas at required RH. The RH was measured at the exit of the flow tube reactor by a humidity probe (HMT330 Sensor, VAISALA, Finland). RH varied between 0 and 90% with ±2% accuracy.

The flow tube reactor is horizontally mounted in a square wooden box. On the upper part of the box, four near-UV lamps (Philips TL-D 18 W, 300−400 nm, length = 60 cm) are mounted perpendicular to the flow tube reactor (Text S1, Figure S1). For these experiments, two lamps were used with a spectral irradiance similar to the sunlight irradiance measured in direct sunlit regions of a typical indoor environment.[23] The emission spectrum of the two lamps was measured with a calibrated spectroradiometer (Ocean Optics, USA) equipped with a linear-array CCD detector (Text S5, Figure S2). The UV absorption spectra of the extracted glass plates were measured by the UV−vis double-beam spectrophotometer (Shanghai Drawell Scientific, China) (Text S4).

NO_x and HONO Measurements. The mixing ratios of NO_2 were measured at the end of the reactor by a chemiluminescence instrument (Eco Physics, model CLD 88p) coupled to a photolytic (metal halide lamp) converter (Eco Physics, model PLC 860). The advantage of the photolytic converter is that it prevents measurement interference from HONO and other NO_y species which is not the case for NO_x instruments using molybdenum converters. The detection limit is 100 ppt, and the time resolution is 1 s.

The HONO mixing ratio was measured using a long-path absorption photometer (LOPAP, QUMA). An external sampling unit is used to sample HONO in an aqueous solution. The mixing ratio of HONO is measured photometrically in a long-path absorption cell after conversion into an azodye which absorbs at 550 nm. The long-path absorption cell is made out of Teflon tubing (Teflon AF2400), which allows light to be transferred in total reflection due to the low refractive index of the Teflon tubing. Under the experimental

https://dx.doi.org/10.1021/acs.est.0c05624
Environ. Sci. Technol. 2020, 54, 15680−15688

conditions (gas flow and pump flow of 1 l min^{-1} and 30 mL min^{-1}, respectively), the detection limit is smaller than 3 ppt with a total accuracy of ±10% with an actual time response of about 5 min and a time resolution of 15 s.[5]

Kinetic Data Treatment. The reactive uptake coefficients of NO_2 with the deposited grime on indoor glass surface were estimated as follows[25]

$$\gamma_{NO_2} = \frac{4 \cdot k_{NO_2}}{\overline{v_{NO_2}}} \frac{V}{S} \quad (1)$$

where k_{NO_2} (s^{-1}) is the pseudo-first-order rate constant for the reaction between NO_2 and the glass plate, S (m^2) is the reactive glass surface, V (m^3) is the volume of the flow tube reactor, and $\overline{v_{NO_2}}$ (m s^{-1}) is the mean molecular speed of NO_2, as given by the bimolecular collision theory

$$\overline{v_{NO_2}} = \sqrt{\frac{8RT}{\pi M}} \quad (2)$$

where R is the ideal gas constant (8.314 J mol^{-1} K^{-1}), T (K) is the absolute temperature, and M = 0.046 (kg mol^{-1}) is the molecular mass of NO_2.

GC−MS Analysis. The glass plates coated with PAHs were analyzed by an Agilent 7890/5975C GC/mass spectrometer detector equipped with a HP-5MS capillary column (30 m, 0.25 mm, and 0.25 mm). High purity helium was used as the carrier gas, with a constant flow rate of 1.2 mL min^{-1}. 1 μL of the sample was injected in a splitless mode with a 6 min solvent delay time using the automated injection device. The GC separation was initiated at 65 °C, held for 2 min, then increased to 290 °C at 5 °C min^{-1} and held for 20 min. PAH compounds were quantified by their authentic standards or approximated with their isomers/homologues closest in retention times as the alternative standards.

The following PAHs were considered for this study: naphthalene (Nap); acenaphthylene (Acey); acenaphthene (Ace); acephenanthrylene (Acepy); fluorene (Fl); phenanthrene (Phe); anthracene (Ant); fluoranthene (Flu); pyrene (Pyr); retene (Ret); benzo(ghi)fluoranthene (Beghif); cyclopenta(cd)pyrene (Cyc); benz(*a*)anthracene (BeA); chrysene/triphenylene (Chr); benzo(b)fluoranthene (BbF); benzo(k)fluoranthene (BkF); benzo(j)fluoranthene (BjF); benzo(e)pyrene (BeP); benzo(a)pyrene (BaP); perylene (Per); indeno(cd)fluoranthene (IcdF); indeno(cd)pyrene (IcdP); dibenzo[*a*,*h*]anthracene (Dib); picene (Pic); benzo(ghi)perylene (BghiP); and coronene (Cor).

Ultra-High-resolution Scanning Electron Microscopy. SEM (HITACHI SU8010, Japan) analysis was performed to investigate the morphology and the microstructure of the exposed glass plates in the kitchen, bedroom, and living room. The glass plates were fixed with conductive adhesive tapes in the sample chamber. SEM analysis of the glass plates required sputter coating of the samples with gold prior to analysis.

Kinetic Modeling. The applied model, KM-SUB[24] in this study was previously described in detail (Text S7). Briefly, the model consists of a gas phase, a sorption layer, a quasi-static surface layer, and several bulk layers. Processes included in the model were reversible adsorption of NO_2, H_2O, HONO, and NO to the indoor surfaces, partitioning of these species between the surface and the bulk, bulk diffusion of all species in the film, and chemical reactions at the surface and in the film bulk. Second-order surface reaction rate coefficients were assumed to equal the bulk reaction rate coefficients multiplied by the thickness of one monolayer. The concentrations of volatile species (NO_2, H_2O, NO, and HONO) in the flow tube ($[X]_g$) were treated as follows[26]

$$\frac{d[X]_g}{dt} = \frac{\phi}{V}([X]_{g,0} - [X]_g) - (J_{ads,X} - J_{des,X})\frac{S}{V} \quad (3)$$

where φ is the volumetric flow rate, V is the volume of the flow tube, $[X]_{g,0}$ is the initial concentration of species X, $J_{ads,X}$ is the adsorption flux of species X, $J_{des,X}$ is the desorption flux of species X, and S is the surface area of the indoor film. Based on measurements, total PAH concentrations used in the model were 3.59×10^{11} cm^{-2} in the kitchen, 1.06×10^{11} cm^{-2} in the bedroom, and 3.18×10^{10} cm^{-2} in the living room.

The following mechanism is included in the model with reactions occurring at the interface and in the bulk of the films

$$\text{PAH or PAH} - \text{OH}(+h\nu) \rightarrow \text{PAH}^* \quad (R1)$$

$$\text{PAH}^* + NO_2 \rightarrow \text{PAH}(+) - NO_2(-) \quad (R2)$$

$$\text{PAH}(+) - NO_2(-) \rightarrow \text{PAH}(+) + NO_2^- \quad (R3)$$

$$NO_2^-(+H^+) \rightarrow \text{HONO} \quad (R4)$$

$$\text{HONO} \rightarrow NO_2^-(+H^+) \quad (R5)$$

$$NO_2^-(+h\nu) \rightarrow \text{NO} + \text{O} \quad (R6)$$

$$\text{PAH}(+) + H_2O \rightarrow \text{PAH} - \text{OH}(+H^+) \quad (R7)$$

$$\text{PAH} - \text{OH} + NO_2^- \rightarrow \text{HONO} + \text{PAH} - O^- \quad (R8)$$

$$\text{PAH} - O^-(+H^+) \rightarrow \text{PAH} - \text{OH} \quad (R9)$$

$$\text{PAH}(+)(+e^-) \rightarrow \text{PAH} \quad (R10)$$

Under UV-A light, the radical cation ($PAHs^+$) can be formed by the electron transfer mechanism from the excited triplet state of PAHs to NO_2. The transfer of an electron from $PAHs^+$ to NO_2 leads to the formation of a charged complex [$PAHs^+$−NO_2^-], which further dissociates back into NO_2^- and $PAHs^+$ (R1−R3). The NO_2^- absorbs UV-A light and yields NO as a byproduct (R4). The acid−base reaction between NO_2^- and H^+ leads to HONO formation (R4). The PAH radical cation forms a PAH−H_2O complex through hydrogen bonding in the presence of water vapors, followed by deprotonation, leading to the formation of PAH−OH (R7). Additionally, PAH−OH can be combined with NO_2^-, leading to the formation of HONO (R8). Reaction 10 is required to maintain a catalytic cycle, even though the exact mechanism is unknown.

Parameters in the model include the thickness of the deposited films, the rate coefficients of reactions R1 and R10, desorption lifetimes, diffusion coefficients, the pH of the films, and partitioning coefficients. The Monte Carlo genetic algorithm (MCGA)[27] was applied to determine a set of parameters, which could reproduce the experimental measurements, and to evaluate model uncertainties, as described in the Supporting Information. Table S3 summarizes the parameter set that leads to the best fitting to the experimental measurements. Although there are many uncertainties in the model, it can help provide insights into some of the observed trends in at least a semiquantitative fashion (Figures S16−S18).

https://dx.doi.org/10.1021/acs.est.0c05624
Environ. Sci. Technol. 2020, 54, 15680−15688

RESULTS AND DISCUSSION

NO_2 and HONO Signals. The heterogeneous reaction of gaseous NO_2 with the solid organic films on the glass surface yields the formation of HONO in the dark and under UV-light irradiation (Figure 1). A decrease of the initial NO_2 mixing ratio (50 ppb) is observed in dark and under light irradiation. This NO_2 value corresponds to the realistic indoor NO_2 mixing ratios in the presence of combustion sources (Figure S12). The formed HONO in the dark is about 2 ppb but rapidly declined over time to 1 ppb. Under UV-light irradiation of the glass plate, HONO increases to 2.5 ppb and decreases slightly to steady state of 2.2 ppb, indicating that PAHs are regenerated leading to a catalytic cycle (see section "Kinetic Modeling").

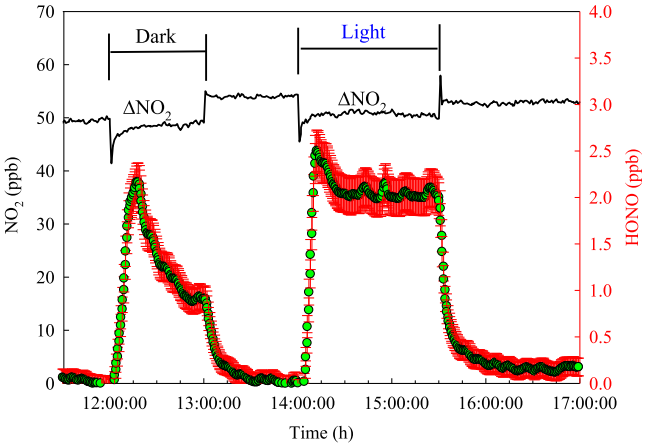

Figure 1. Signal of NO_2 uptake in the dark and under light irradiation on the glass of the kitchen. The formation of HONO (green dots) in the dark and under light irradiation of the glass window of the kitchen at a 50 ppb initial mixing ratio of NO_2 at 60% RH. The error bars (red) correspond to the 10% uncertainties in the measurements of HONO by LOPAP.

Speculatively, slow transport of PAHs toward the surface can be the reason for the observed steady state of HONO in Figure 1.

Reactive Uptake Coefficients of NO_2. The reactive uptake coefficients of NO_2, $\gamma(NO_2)$, on the glass covered with organic films were investigated as a function of RH at 296 K in the dark and under UV-A light irradiation ($300 < \lambda < 400$ nm). The Langmuir–Hinshelwood behavior of the uptake coefficients under light irradiation is shown in Figure S5.

In darkness, $\gamma(NO_2)$ on the glass window from the kitchen exhibit linear dependence with RH (Figure S3). $\gamma(NO_2)$ on the glass windows from the bedroom and living room under dark conditions were close to the detection limit $\approx 10^{-8}$.[25]

In the presence of UV-light (8 W m^{-2} for $300 < \lambda < 400$ nm), $\gamma(NO_2)$ on both the living room and bedroom window glass increase 1 order of magnitude from 1.5×10^{-7} at 0% RH to about 1.5×10^{-6} at 90% RH (Figure 2). On the kitchen window glass, $\gamma(NO_2)$ are already higher at 2.3×10^{-6}, compared to $\gamma(NO_2)$ on bedroom and living room at 0% RH, and increase up to 4.1×10^{-6} at 90% RH. $\gamma(NO_2)$ on the kitchen window glass are the same order of magnitude as the $\gamma(NO_2)$ on urban grime adsorbed on a glass window in downtown Guangzhou [$\gamma(NO_2) = (1.1 \pm 0.2) \times 10^{-6}$ at 0% RH and $(5.8 \pm 0.7) \times 10^{-6}$ at 90% RH] obtained at a similar initial NO_2 mixing ratio of 50 ppb but two times stronger light irradiation.[25] The increase of $\gamma(NO_2)$ on glass plates from the kitchen, with light intensity is shown in the Supporting Information (Figure S4). The enhanced $\gamma(NO_2)$ under UV-A light irradiation can be ascribed to the adsorbed PAHs on glass surfaces, which originate mostly from cooking activities.[21] These PAHs, namely, fluorene, phenanthrene, fluoranthene, and pyrene absorb UV-A light in the range of wavelengths that are available indoors,[3−5,23] which can act as photosensitizers after photoactivation[28,29] to induce higher $\gamma(NO_2)$ on humidified surfaces[30] (see R1−R10). However, the reported $\gamma(NO_2)$ on pure solid films consisting of PAHs were lower than the $\gamma(NO_2)$ on the kitchen glass window from this study. For example, the highest $\gamma(NO_2)$ were observed on solid films of fluoranthene (1.07×10^{-6}),[29] phenanthrene (1.34×10^{-6}),[29] and pyrene (3.2×10^{-6}),[36] which are still lower than $\gamma(NO_2)$ on the kitchen glass at higher RH (about 80%).

While the organic film on the glass efficiently eliminates gas-phase NO_2, it gives rise to the gaseous reaction products of NO and HONO, as shown in Figure 3. The NO and HONO

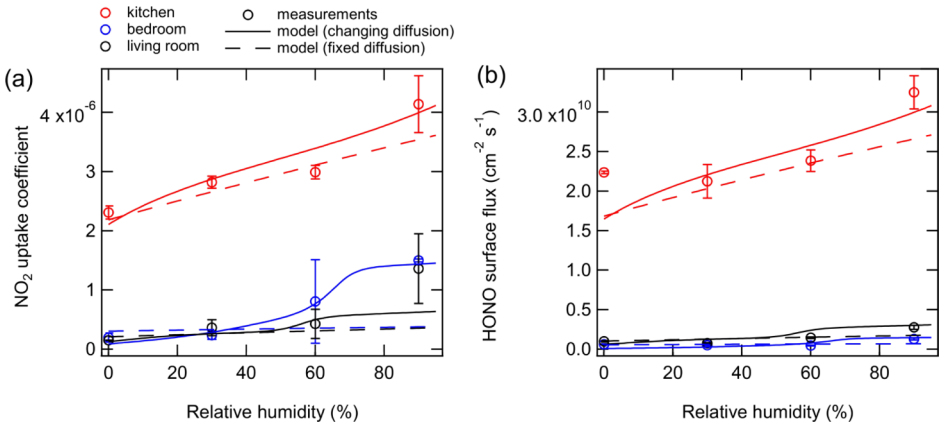

Figure 2. (a) NO_2 uptake coefficients and (b) HONO surface fluxes as a function of RH at 296 K in the presence of light (8 W m^{-2} for $300 < \lambda < 400$ nm) in the kitchen (red), bedroom (blue), and living room (black). The HONO surface fluxes correspond to initial NO_2 mixing ratios of 50 ppb. Markers represent experimental measurements, while lines represent model outputs with changing bulk diffusion coefficients as a function of RH (solid) or with constant bulk diffusion coefficients (dashed). The error bars are derived from the uncertainties associated to the estimation of the uptake coefficients. Error bars of HONO surface flux indicate the standard deviation from three independent measurements.

https://dx.doi.org/10.1021/acs.est.0c05624
Environ. Sci. Technol. 2020, 54, 15680−15688

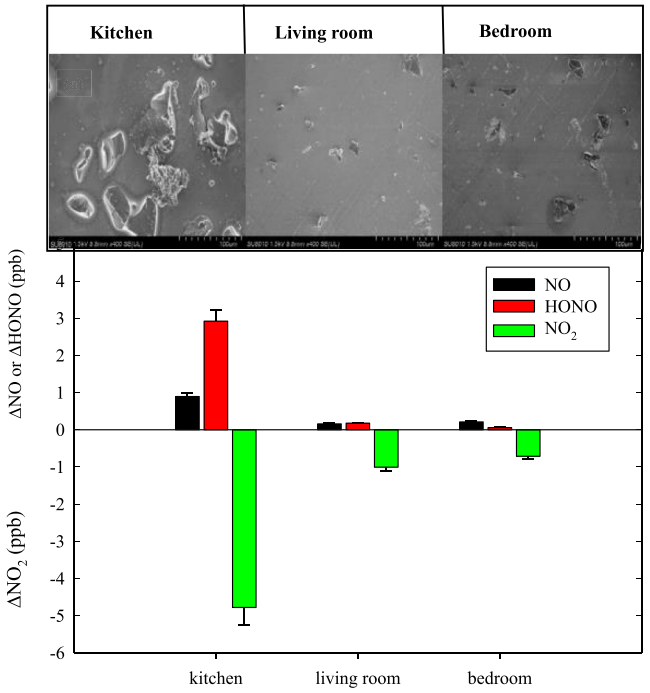

Figure 3. NO_2 loss, NO and HONO formation by the glass window surface at a NO_2 mixing ratio of 50 ppb and RH of 50%. Error bars indicate the standard deviation from three independent measurements. The upper panel is the UHR-SEM image of the glass window from the (a) kitchen, (b) living room, and (c) bedroom (noncontact mode, 100 μm scanner).

yields are higher for the kitchen glass than for the living room and bedroom. Both gas-phase pollutants (NO and HONO) are formed most plausibly by the reaction mechanism which has been suggested in previous studies.[28,29] Exposure of the glass plates to all three indoor locations caused deposition of the larger sized particles, the most significant in the kitchen[31] (Figure 3). Cooking emissions tend to form smoother hills of coatings,[31] aggregated organic compounds emerging from smaller organic species during the sampling period of 1 month. As displayed in Figures 3 and S15, the particles are unevenly distributed over the glass plates with irregular morphologies and diverse particle shapes and sizes in all three cases. It must be stressed that there is a big difference between the glass from the kitchen and the other two samples from the bedroom and living room, the particles are larger and more densely packed on the kitchen glass. Cooking activities release a variety of organic compounds, which may induce the formation of organic films on indoor surfaces containing cooking oils (triglycerides) and PAHs.[32] The total concentrations of 26 PAHs adsorbed on the glass in the kitchen, living room, and bedroom, analyzed by GC−MS, are summarized in Table S1 (Text S6). Figure S6 shows, in a graphical manner, the concentration of the PAHs on the glass surface in the kitchen, living room, and the bedroom. Clearly, the high PAH concentrations in the kitchen emerge from the cooking activities. To our best, we do not have an explanation for the variation of PAH concentrations between the living room and bedroom but one hypothesis is the different air exchange rates, and this should be further explored. Figures S7−S10 show the total ion chromatograms for the samples from kitchen, bedroom, living room, and PAH standard samples, respectively. The area-normalized concentrations of total PAHs on the glass window from the kitchen were much higher, 1132 ng/m^2, compared to the glass samples in bedroom and living room, 299 and 93 ng/m^2, respectively, in agreement with the literature data from other locations in the world (see the text 6 in the Supporting Information).[33,34] The concentrations of PAHs on the glass surfaces from the kitchen, bedroom, and living room explain the magnitude of NO_2 loss in Figure 3: the highest ΔNO_2 was observed on the glass from the kitchen followed by the similar NO_2 consumption on the glass from bedroom and living room. The PAHs emitted from combustion are adsorbed on the glass window and most likely drive the formation of high HONO yields on the kitchen glass through photosensitized processes between the electronically excited triplet state of PAHs and co-adsorbed NO_2 on the glass surface (R1−R10).

It has to be noted that the glass plates collected from the kitchen contain anions (see Table S2) which may inhibit the NO_2 to HONO conversion.[35] Because the glass plates were not pretreated, the presented uptake coefficients in Figure 2 already show the effect of inorganic ions on the heterogeneous reactivity.

HONO Yields. The conversion yields of HONO and NO were estimated as $\Delta HONO/\Delta NO_2$ and $\Delta NO/\Delta NO_2$, respectively, where ΔNO_2 is the difference between initial and final NO_2 mixing ratios in ppb, and ΔNO and $\Delta HONO$ are the formed quantities of NO and HONO. Table 1 summarizes the HONO and NO yields produced by heterogeneous conversion of NO_2 on glass windows in a kitchen, living room, and bedroom at different RH. There is slight variation of HONO yields with RH for all three scenarios, but they are much higher for the kitchen ranging between 61% at RH 60 and 78% under dry conditions. The NO yields were much lower compared to the HONO yields ranging between 10 and 30% for all of the three different scenarios. Interestingly, for the kitchen glass, the sum of both NO and HONO yields at RH 0 and 30% was almost 100%, indicating complete conversion of NO_2 to gaseous NO and HONO. At RH 60 and 90%, the sum of the NO and HONO yields was smaller than those at RH 0 and 30%, but still as high as those at RH 80%, confirming the catalytic role of adsorbed PAHs on the kitchen glass window (R1−R10). For the

Table 1. HONO and NO Conversion Yields at Different RH[a]

	kitchen			living room			bedroom		
RH (%)	HONO yield (%)	NO yield (%)	ΔNO_2	HONO yield (%)	NO yield (%)	ΔNO_2	HONO yield (%)	NO yield (%)	ΔNO_2
0	78.4	18.3	3.1	13.4	21.9	0.9	12.7	21.4	0.6
30	70.0	26.7	3.7	7.0	20.0	1.6	22.2	12.5	0.3
60	61.1	18.7	4.8	9.6	15.7	1.8	7.9	29.6	0.7
90	64.4	10.2	6.2	14.7	11.4	2.3	24.5	26.2	0.6

[a]The initial NO_2 mixing ratio is 50 ppb with light irradiation 8 W m^{-2} for 300 < λ < 400 nm.

https://dx.doi.org/10.1021/acs.est.0c05624
Environ. Sci. Technol. 2020, 54, 15680−15688

bedroom and living room, the sum of the HONO and NO yields was much smaller ranging between 30 and 40%.

The NO_2 to HONO conversion yields of 80% were previously reported on an urban grime[25] and humic acid.[36] To the best of our knowledge, this is the first time such high HONO yields have been observed in an indoor scenario under attenuated UV-light intensity (8 W m^{-2} for $300 < \lambda < 400$ nm) highlighting light-induced heterogeneous NO_2 conversion on indoor surfaces as an important HONO source in indoor air.

From the HONO concentration measurements, the HONO surface fluxes were estimated by a procedure described in the Supporting Information (text S9) and the obtained values are shown in Figure 2 and compared with the kinetic model.

Comparison of Kinetic Modeling with Laboratory Experiments. Kinetic modeling reproduce experimental measurements of NO_2 uptake coefficients and HONO surface fluxes reasonably well (Figure 2). Several key features of these measurements can be better understood from the model. NO_2 uptake coefficients were highest for the kitchen films and lowest for the living room films, reflecting that these films contained the highest and lowest number of PAH molecules, respectively. It was necessary to apply higher photo-excitation rates of PAH or PAH-OH compared to our calculated value of 4.8×10^{-2} s^{-1}. If a value of 4.8×10^{-2} s^{-1} was used, the uptake coefficients could not be reproduced and NO_2 uptake coefficients became limited by the availability of PAH*. This suggests that either the PAH products may have a larger absorption cross-section than the PAH itself or that photon scattering may be occurring on the surface. This result is consistent with previous studies that have observed higher photolysis rates on surfaces.[37,38] Note that the existence of other chromophores such as oxy-PAHs on the glass plates could possibly help to better fit the experimental data with the model.

The results also suggest that phase state and bulk diffusivity play important roles in the NO_2 uptake. The dashed lines in Figure 2 represent the best fit to the measurements that was obtained with fixed diffusion coefficients, while the solid lines represent diffusion coefficients changing as a function of RH. With fixed diffusion coefficients, the measurements in the kitchen could be fairly well reproduced, with $\gamma(NO_2)$ increasing with increasing RH due to reaction R7; however, the model is unable to reproduce the large increase in $\gamma(NO_2)$ at 90% RH in the bedroom and living room. With changing diffusion coefficients as a function of RH, the uptake was controlled by the surface reaction which was limited by the diffusion rate of PAH* to the surface. The estimated diffusion coefficients were consistent with solid or semisolid films at low RH transitioning to semisolid or liquid films at higher RH.[39] The estimated film thicknesses of 4−41 nm are consistent with some recent publications.[17,40,41] Although NO_2 uptake coefficients in the living room and bedroom were similar, the HONO fluxes in the living room were slightly higher than in the bedroom. It can be speculated that this could be due to the pH of the film and the conversion rate of NO_2^- to HONO (reaction R4). The measurements could only be reproduced by allowing the rate coefficient of this reaction to vary for the different films. HONO yields outputted from the model were ∼74, ∼9, ∼43% in the kitchen, bedroom, and living room, respectively, and did not change significantly as a function of RH, suggesting that the reaction pathway may not be as important as the phase state for this particular reaction system. However, note that there are uncertainties and simplifications in the model and that it could be further refined in future studies if more parameters could be constrained.

Implications for Indoor Air Quality. A dynamic mass balance[12−14] can be used to simulate the formation of HONO by light-induced heterogeneous NO_2 conversion on a glass window of the kitchen. We can consider the size of the kitchen to be 2.5 m high, 3 m wide, and 4 m long, hence with a total volume of 30 m^3 which corresponds to the size of the kitchen where the glass plates were placed during a 1-month period and used for these experiments. Considering that the surface of the window is 4 m^2 and assuming an initial NO_2 mixing ratio of 50 ppb and 60% RH, the HONO emission rate (E_R) in the dark is estimated as 0.1 mg h^{-1} based on the HONO data shown in Figure 1 and the procedure described in Text S9. The generated HONO mixing ratio $c_a(t)$ under attenuated UV-light conditions can be estimated as follows

$$c_a(t) = \frac{E_R}{k_{AER} V} + \left(c_0 - \frac{E_R}{k_{AER} V}\right) e^{-(k_{AER} t)} \quad (4)$$

where E_R is the emission rate of HONO (mg h^{-1}), c_0 is the initial HONO concentration (mg m^{-3}) assumed to be zero at $t = 0$, t is the time (h), $V = 30$ m^3 is the volume of the kitchen, and $k_{AER} = 0.56$ h^{-1} is the average air exchange rate.[42] To test the sensitivity of the model, we also modeled the HONO formation under two extreme conditions assuming airtight room with $k_{AER} = 0.1$ h^{-1} and well-ventilated room with $k_{AER} = 0.9$ h^{-1}. These values would also correspond to reality because in a long-term study, different indoor environments had k_{AER} values ranging from 0.29 to 3.46 h^{-1} in fall and 0.12 to 1.39 h^{-1} in winter.[43] The homes had a median $k_{AER} = 1.15$ h^{-1} in fall and 0.54 h^{-1} in winter.[43] The measured k_{AER} in this study are reported in the Supporting Information (Text S8, Figure S11).

The window of the kitchen is exposed to the direct sunlight of 8 W m^{-2} ($330 < \lambda < 400$ nm) during certain periods of the day. Based on the measured spectral irradiance near the glass window in the kitchen, the photolysis rate of HONO, $J(HONO)$, is summarized in Table S4.[5] During this period, the conversion of NO_2 on the glass window is enhanced by the UV-light, leading to higher HONO yields (Figure 1) than in the dark. Under these conditions, the HONO emission rate produced by the light-induced heterogeneous reaction of 50 ppb of NO_2 with the glass window at 60% RH is 0.24 mg h^{-1}. It has to be noted that although the uptake coefficients increase with the light intensity (Figure S4), we considered HONO values formed in the dark, 0.1 mg h^{-1}, and in the presence of light, 0.24 mg h^{-1} (8 W m^{-2} for $300 < \lambda < 400$ nm). This HONO value is a conservative value because the stronger light intensity can induce higher HONO values. However, we use only two HONO values (dark and light) in the model because even if we measure the HONO yields formed under different light intensities, these values would not correspond to the real variation of the light intensity indoors. The generated HONO mixing ratio $c_a(t)$ by light-induced conversion of NO_2 on the glass window in the kitchen is given as follows

$$c_a(t) = \frac{E_R}{k_{AER} V + J(HONO) V_1} + \left(c_0 - \frac{E_R}{k_{AER} V + J(HONO) V_1}\right) e^{-(k_{AER} + J(HONO))t} \quad (5)$$

https://dx.doi.org/10.1021/acs.est.0c05624
Environ. Sci. Technol. 2020, 54, 15680−15688

where V_1 is the volume of the air in the sunlit kitchen when HONO is photolyzed, assumed to be 1/3 of the total volume of the kitchen, (V) = 30 m^3.

Figure 4 shows the continuous HONO production during 24 h induced by NO_2 heterogeneous chemistry on glass windows. The estimated changing HONO mixing ratio generated by NO_2 conversion on the glass window of the kitchen under attenuated light conditions and in the sunlit kitchen is depicted in Figure 4. At average k_{AER} = 0.56 h^{-1}, the HONO production in the dark remains stable, ca. 3 ppb, from 1 to 8 o'clock in the morning. The first sunbeams in the morning around 8 o'clock cause an increase of HONO from 3 to 7 ppb from 8 to 9 o'clock because of light-induced heterogeneous conversion of NO_2 on the glass window, which remains stable, ca. 7, ppb until 11 o'clock. In the period from 11 to 13 o'clock because of intense sunlight activity, the enhanced HONO formation is compensated with HONO photolysis which leads to a decrease of HONO from 7 to 5.5 ppb. From 13 to 19 o'clock, the HONO remains stable around 7 ppb which then again decreases to 3 ppb from 20 o'clock to midnight. The estimated HONO values through heterogeneous NO_2 conversion on glass windows in the living room and bedroom are shown in the Supporting Information (Figures S13 and S14). For these estimations, we assumed the same J(HONO) values as in the kitchen although the different orientation of these two rooms would imply different J(HONO) values.

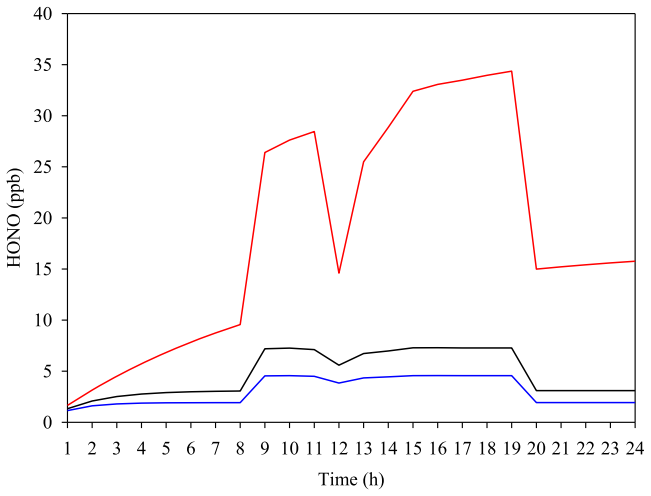

Figure 4. Modeled HONO values generated by NO_2 conversion on a window glass of the kitchen in the absence of direct sunlight irradiation and under light irradiation of the glass window at air exchange rate (AER) = 0.5 h^{-1} (black line), AER = 0.9 h^{-1} (blue line), and AER = 0.1 h^{-1} (red line). The experimental conditions used for the model estimations are depicted in the Supporting Information.

These results indicate that HONO is continuously formed in the indoor environment upon heterogeneous conversion of NO_2 on the glass windows. In particular, HONO is rapidly formed during the irradiation of the windows by sunlight. The model did not consider HONO yields formed under different light intensity. This explains the sharp decrease of modeled HONO at noon due to its photolysis. Considering a HONO value formed under stronger light intensity would likely recompense this fall. Thus, an improvement of this model or development of models to accurately predict the HONO values under different light intensities are highly recommended. It has to be noted that HONO can also be deposited to the indoor surfaces, but this was not considered in the model.

The high HONO yields observed during the irradiation period of the glass windows in the kitchen have strong repercussions for indoor air quality as HONO is a harmful pollutant and is also readily photolyzed yielding high amounts of OH radicals in indoor air,[3−5] which can further react and form a myriad of secondary gas-phase products,[22] among which some can be potentially hazardous for human health.

■ ASSOCIATED CONTENT

Supporting Information

The Supporting Information is available free of charge at https://pubs.acs.org/doi/10.1021/acs.est.0c05624.

Additional text about the experimental setup, sampling procedure, anions analysis, UV absorption spectra, spectral irradiance, PAHs analysis, MCGA simulations, estimation of AER, and estimation of HONO surface flux; uptake coefficients of NO_2 on a kitchen glass in dark as a function of RH; uptake coefficients of NO_2 on a glass plate from the kitchen as a function of the initial NO_2 mixing ratios under light irradiation; uptake coefficients of NO_2 on a kitchen glass as a function of light intensity; PAH composition of the organic film on the glass plates in the kitchen, bedroom, and living room; typical signal of NO_2 during the cooking event in the kitchen where the glass plates were deposited; modeled HONO values generated by NO_2 conversion on a window glass of the living room and bedroom in the absence of direct sunlight irradiation and under light irradiation of the glass window; SEM image of the glass plates from the kitchen, living room, and bedroom; box whisker plots of the ranges of partitioning coefficient desorption lifetimes and film thicknesses outputted from the MCGA; box whisker plots of the diffusion coefficient ranges outputted from the MCGA; box whisker plots of the rate coefficient ranges outputted from the MCGA; total concentrations of PAHs adsorbed on glass in kitchen, bedroom, and living room; concentration of the major anions measured in the glass plates from the kitchen; parameters used in the KM-SUB model; and photolysis frequencies of HONO during 24 h (PDF)

■ AUTHOR INFORMATION

Corresponding Authors

Manabu Shiraiwa − *Department of Chemistry, University of California, Irvine, Irvine, California 92697-2025, United States;* orcid.org/0000-0003-2532-5373; Email: m.shiraiwa@uci.edu

Sasho Gligorovski − *State Key Laboratory of Organic Geochemistry, Guangdong Provincial Key Laboratory of Environmental Protection and Resources Utilization, and Guangdong–Hong Kong–Macao Joint Laboratory for Environmental Pollution and Control, Guangzhou Institute of Geochemistry, Chinese Academy of Sciences, Guangzhou 510640, China;* orcid.org/0000-0003-4151-2224; Email: gligorovski@gig.ac.cn

Authors

Jiangping Liu − *State Key Laboratory of Organic Geochemistry, Guangzhou Institute of Geochemistry, Chinese*

https://dx.doi.org/10.1021/acs.est.0c05624
Environ. Sci. Technol. 2020, 54, 15680−15688

Academy of Sciences, Guangzhou 510640, China
Huifan Deng − *State Key Laboratory of Organic Geochemistry, Guangzhou Institute of Geochemistry, Chinese Academy of Sciences, Guangzhou 510640, China; University of Chinese Academy of Sciences, Beijing 100049, China*
Pascale S. J. Lakey − *Department of Chemistry, University of California, Irvine, Irvine, California 92697-2025, United States*
Haoyu Jiang − *State Key Laboratory of Organic Geochemistry, Guangzhou Institute of Geochemistry, Chinese Academy of Sciences, Guangzhou 510640, China*
Majda Mekic − *State Key Laboratory of Organic Geochemistry, Guangzhou Institute of Geochemistry, Chinese Academy of Sciences, Guangzhou 510640, China; University of Chinese Academy of Sciences, Beijing 100049, China*
Xinming Wang − *State Key Laboratory of Organic Geochemistry, Guangdong Provincial Key Laboratory of Environmental Protection and Resources Utilization, and Guangdong–Hong Kong–Macao Joint Laboratory for Environmental Pollution and Control, Guangzhou Institute of Geochemistry, Chinese Academy of Sciences, Guangzhou 510640, China;* orcid.org/0000-0002-1982-0928

Complete contact information is available at: https://pubs.acs.org/10.1021/acs.est.0c05624

Author Contributions

J.L. and P.S.J.L. contributed equally to this work. S.G. and M.S. designed research. J.L. and H.D. performed the laboratory experiments. P.S.J.L. and M.S. performed the kinetic modeling. J.L., H.D., H.J., and M.M. analyzed and interpreted the data from laboratory experiments. X.W. contributed to the data analysis and relevant discussion in the Supporting Information. S.G., P.S.J.L., and M.S. wrote the manuscript with input from all coauthors.

Funding

This study was financially supported by the National Key Research and Development Program (2017YFC0210103), the National Natural Science Foundation of China (41773131 and 41977187), the State Key Laboratory of Organic Geochemistry, Guangzhou Institute of Geochemistry (SKLOG2020-5 and KTZ_17101), and Chinese Academy of Sciences, International Cooperation Grant (132744KYSB20190007). The modeling work is funded by the Alfred P. Sloan Foundation (G-2019-12306).

Notes

The authors declare no competing financial interest.
All data needed to evaluate the conclusions in the paper are present in the paper and/or the Supporting Information. Additional data related to this paper may be requested from the authors.

■ ACKNOWLEDGMENTS

P.S.J.L. and M.S. thank T. Berkemeier for sharing the code of the MCGA.

■ REFERENCES

(1) Pitts, J. N., Jr.; Grosjean, D.; Van Cauwenberghe, K.; Schmid, J. P.; Fitz, D. R. Photooxidation of aliphatic amines under simulated atmospheric conditions: formation of nitrosamines, nitramines, amides and photochemical oxidant. *Environ. Sci. Technol.* **1978**, *12*, 946−953.
(2) Sleiman, M.; Gundel, L. A.; Pankow, J. F.; Jacob, P.; Singer, B. C.; Destaillats, H. Formation of carcinogens indoors by surface-mediated reactions of nicotine with nitrous acid, leading to potential thirdhand smokehazards. *Proc. Natl. Acad. Sci. U.S.A.* **2010**, *107*, 6576−6581.
(3) Gómez Alvarez, E.; Amedro, D.; Afif, C.; Gligorovski, S.; Schoemaecker, C.; Fittschen, C.; Doussin, J.-F.; Wortham, H. Photolysis of nitrous acid as a primary source of OH radicals indoors. *Proc Natl. Acad. Sci. U.S.A.* **2013**, *110*, 13294−13299.
(4) Zhou, S.; Young, C. J.; VandenBoer, T. C.; Kowal, S. F.; Kahan, T. F. Time-Resolved Measurements of Nitric Oxide, Nitrogen Dioxide, and Nitrous Acid in an Occupied New York Home. *Environ. Sci. Technol.* **2018**, *52*, 8355−8364.
(5) Liu, J.; Li, S.; Zeng, J.; Mekic, M.; Yu, Z.; Zhou, W.; Loisel, G.; Gandolfo, A.; Song, W.; Wang, X.; Zhou, Z.; Herrmann, H.; Li, X.; Gligorovski, S. Assessing indoor gas phase oxidation capacity through real-time measurements of HONO, NOx and ozone in Guangzhou, China. *Environ. Sci. Processes. Impacts* **2019**, *21*, 1393−1402.
(6) Gligorovski, S. Nitrous acid (HONO): An emerging indoor pollutant. *J. Photochem. Photobiol., A* **2016**, *314*, 1−5.
(7) Vecera, Z.; Dasgupta, P. K. Indoor Nitrous Acid Levels. Production of Nitrous Acid from Open-Flame Sources. *Int. J. Environ. Clim. Change* **1994**, *56*, 311−316.
(8) Bartolomei, V.; Gomez Alvarez, E.; Wittmer, J.; Tlili, S.; Strekowski, R.; Temime-Roussel, B.; Quivet, E.; Wortham, H.; Zetzsch, C.; Kleffmann, J.; Gligorovski, S. Combustion processes as a source of high levels of indoor hydroxyl radical (OH) through the photolysis of nitrous acid (HONO). *Environ. Sci. Technol.* **2015**, *49*, 6599−6607.
(9) Collins, D. B.; Hems, R. F.; Zhou, S.; Wang, C.; Grignon, E.; Alavy, M.; Siegel, J. A.; Abbatt, J. P. D. Evidence for Gas-Surface Equilibrium Control of Indoor Nitrous Acid. *Environ. Sci. Technol.* **2018**, *52*, 12419−12427.
(10) Sakamaki, F.; Hatakeyama, S.; Akimoto, H. Formation of nitrous acid and nitric oxide in the heterogeneous dark reaction of nitrogen dioxide and water vapor in a smog chamber. *Int. J. Chem. Kinet.* **1983**, *15*, 1013−1029.
(11) Finlayson-Pitts, B. J.; Wingen, L. M.; Sumner, A. L.; Syomin, D.; Ramazan, K. A. The heterogeneous hydrolysis of NO_2 in laboratory systems and in outdoor and indoor atmospheres: An integrated mechanism. *Phys. Chem. Chem. Phys.* **2003**, *5*, 223−242.
(12) Gómez Alvarez, E.; Sörgel, M.; Gligorovski, S.; Bassil, S.; Bartolomei, V.; Coulomb, B.; Zetzsch, C.; Wortham, H. Light-induced nitrous acid (HONO) production from NO_2 heterogeneous reactions on household chemicals. *Atmos. Environ.* **2014**, *95*, 391−399.
(13) Bartolomei, V.; Sörgel, M.; Gligorovski, S.; Alvarez, E. G.; Gandolfo, A.; Strekowski, R.; Quivet, E.; Held, A.; Zetzsch, C.; Wortham, H. Formation of indoor nitrous acid (HONO) by light-induced NO_2 heterogeneous reactions with white wall paint. *Environ. Sci. Pollut. Res.* **2014**, *21*, 9259−9269.
(14) Gandolfo, A.; Bartolomei, V.; Gomez Alvarez, E.; Tlili, S.; Gligorovski, S.; Kleffmann, J.; Wortham, H. The effectiveness of indoor photocatalytic paints on NO_x and HONO levels. *Appl. Catal., B* **2015**, *166−167*, 84−90.
(15) Lee, K.; Xue, J.; Geyh, A. S.; Özkaynak, H.; Leaderer, B. P.; Weschler, C. J.; Spengler, J. D. Nitrous Acid, nitrogen dioxide, and ozone concentrations in residential environments. *Environ. Health Perspect.* **2002**, *110*, 145−150.
(16) Weschler, C. J. Changes in indoor pollutants since the 1950s. *Atmos. Environ.* **2009**, *43*, 153−169.
(17) Weschler, C. J.; Nazaroff, W. W. Growth of organic films on indoor surfaces. *Indoor Air* **2017**, *27*, 1101−1112.
(18) Tamas, G.; Weschler, C.; Bakobiro, Z.; Wyon, D.; Stromtejsen, P. Factors affecting ozone removal rates in a simulated aircraft cabin environment. *Atmos. Environ.* **2006**, *40*, 6122−6133.
(19) Fang, Y.; Lakey, P. S. J.; Riahi, S.; McDonald, A. T.; Shrestha, M.; Tobias, D. J.; Shiraiwa, M.; Grassian, V. H. A molecular picture of surface interactions of organic compounds on prevalent indoor

surfaces: limonene adsorption on SiO_2. *Chem. Sci.* **2019**, *10*, 2906−2914.
(20) Zhou, S.; Yeung, L. W. Y.; Forbes, M. W.; Mabury, S.; Abbatt, J. P. D. Epoxide formation from heterogeneous oxidation of benzo[a]-pyrene with gas-phase ozone and indoor air. *Environ. Sci.: Processes Impacts* **2017**, *19*, 1292−1299.
(21) Wu, M.-T.; Lin, P. C.; Pan, C. H.; Peng, C. Y. Risk assessment of personal exposure to polycyclic aromatic hydrocarbons and aldehydes in three commercial cooking workplaces. *Sci. Rep.* **2019**, *9*, 1661−1672.
(22) Zeng, J.; Yu, Z.; Mekic, M.; Liu, J.; Li, S.; Loisel, G.; Gao, W.; Gandolfo, A.; Zhou, Z.; Wang, X.; Herrmann, H.; Gligorovski, S.; Li, X. Evolution of indoor cooking emissions captured by using secondary electrospray ionization high resolution mass spectrometry. *Environ. Sci. Technol. Lett.* **2020**, *7*, 76−81.
(23) Gandolfo, A.; Gligorovski, V.; Bartolomei, V.; Tlili, S.; Gómez Alvarez, E.; Wortham, H.; Kleffmann, J.; Gligorovski, S. Spectrally resolved actinic flux and photolysis frequency of key species within indoor environment. *Build. Environ.* **2016**, *109*, 50−57.
(24) Shiraiwa, M.; Pfrang, C.; Pöschl, U. Kinetic multi-layer model of aerosol surface and bulk chemistry (KM-SUB): the influence of interfacial transport and bulk diffusion on the oxidation of oleic acid by ozone. *Atmos. Chem. Phys.* **2010**, *10*, 3673−3691.
(25) Liu, J.; Li, S.; Mekic, M.; Jiang, H.; Zhou, W.; Loisel, G.; Song, W.; Wang, X.; Gligorovski, S. Photoenhanced Uptake of NO_2 and HONO Formation on Real Urban Grime. *Environ. Sci. Technol. Lett.* **2019**, *6*, 413−417.
(26) Berkemeier, T.; Steimer, S. S.; Krieger, U. K.; Peter, T.; Pöschl, U.; Ammann, M.; Shiraiwa, M. Ozone uptake on glassy, semi-solid and liquid organic matter and the role of reactive oxygen intermediates in atmospheric aerosol chemistry. *Phys. Chem. Chem. Phys.* **2016**, *18*, 12662−12674.
(27) Berkemeier, T.; Ammann, M.; Krieger, U. K.; Peter, T.; Spichtinger, P.; Pöschl, U.; Shiraiwa, M.; Huisman, A. J. Technical note: Monte Carlo genetic algorithm (MCGA) for model analysis of multiphase chemical kinetics to determine transport and reaction rate coefficients using multiple experimental data sets. *Atmos. Chem. Phys.* **2017**, *17*, 8021−8029.
(28) Brigante, M.; Cazoir, D.; D'Anna, B.; George, C.; Donaldson, D. J. Photoenhanced Uptake of NO_2 by Pyrene Solid Films. *J. Phys. Chem. A* **2008**, *112*, 9503−9508.
(29) Cazoir, D.; Brigante, M.; Ammar, R.; D'Anna, B.; George, C. Heterogeneous Photochemistry of Gaseous NO_2 on Solid Fluoranthene Films: A Source of Gaseous Nitrous Acid (HONO) in the Urban Environment. *J. Photochem. Photobiol., A* **2014**, *273*, 23−28.
(30) George, C.; Strekowski, R. S.; Kleffmann, J.; Stemmler, K.; Ammann, M. Photoenhanced uptake of gaseous NO_2 on solid organic compounds: a photochemical source of HONO? *Faraday Discuss.* **2005**, *130*, 195−210.
(31) Or, V. W.; Alves, M. R.; Wade, M.; Schwab, S.; Corsi, R. L.; Grassian, V. H. Crystal Clear? Microspectroscopic Imaging and Physicochemical Characterization of Indoor Depositions on Window Glass. *Environ. Sci. Technol. Lett.* **2018**, *5*, 514−519.
(32) Zhou, S.; Hwang, B. C. H.; Lakey, P. S. J.; Zuend, A.; Abbatt, J. P. D.; Shiraiwa, M. Multiphase reactivity of polycyclic aromatic hydrocarbons is driven by phase separation and diffusion limitations. *Proc. Natl. Acad. Sci. U.S.A.* **2019**, *116*, 11658−11663.
(33) Pan, S.-H.; Li, J.; Lin, T.; Zhang, G.; Li, X.-D.; Yin, H. Polycyclic aromatic hydrocarbons on indoor/outdoor glass window surfaces in Guangzhou and Hong Kong, south China. *Environ. Pollut.* **2012**, *169*, 190−195.
(34) Duigu, J. R.; Ayoko, G. A.; Kokot, S. The relationship between building characteristics and the chemical composition of surface films found on glass windows in Brisbane, Australia. *Build. Environ.* **2009**, *44*, 2228−2235.
(35) Liu, J.; Deng, H.; Li, S.; Jiang, H.; Mekic, M.; Zhou, W.; Wang, Y.; Loisel, G.; Wang, X.; Gligorovski, S. Light-Enhanced Heterogeneous Conversion of NO_2 to HONO on Solid Films Consisting of Fluorene and Fluorene/Na_2SO_4: An Impact on Urban and Indoor Atmosphere. *Environ. Sci. Technol.* **2020**, *54*, 11079−11086.
(36) Stemmler, K.; Ammann, M.; Donders, C.; Kleffmann, J.; George, C. Photosensitized reduction of nitrogen dioxide on humic acid as a source of nitrous acid. *Nature* **2006**, *440*, 195−198.
(37) Xu, C.; Dong, D.; Meng, X.; Su, X.; Zheng, X.; Li, Y. Photolysis of polycyclic aromatic hydrocarbons on soil surfaces under UV irradiation. *J. Environ. Sci.* **2013**, *25*, 569−575.
(38) Kahan, T. F.; Donaldson, D. J. Photolysis of polycyclic aromatic hydrocarbons on water and ice surfaces. *J. Phys. Chem. A* **2007**, *111*, 1277−1285.
(39) Shiraiwa, M.; Ammann, M.; Koop, T.; Pöschl, U. Gas uptake and chemical aging of semisolid organic aerosol particles. *Proc. Natl. Acad. Sci. U.S.A.* **2011**, *108*, 11003−11008.
(40) Deming, B. L.; Ziemann, P. J. Quantification of alkenes on indoor surfaces and implications for chemical sources and sinks. *Indoor Air*, **2020**, *30*, doi.org/ DOI: 10.1111/ina.12662.
(41) Or, V. W.; Wade, M.; Patel, S.; Alves, M. R.; Kim, D.; Schwab, S.; Przelomski, H.; O'Brien, R.; Rim, D.; Corsi, R. L.; Vance, M. E.; Farmer, D. K.; Grassian, V. H. Glass surface evolution following gas adsorption and particle deposition from indoor cooking events as probed by microspectroscopic analysis. *Environ. Sci.: Processes Impacts* **2019**, *22*, 1698−1709.
(42) Wallace, L. A.; Emmerich, S. J.; Howard-Reed, C. Continuous measurements of air change rates in an occupied house for 1 year: The effect of temperature, wind, fans, and windows. *J. Exposure Sci. Environ. Epidemiol.* **2002**, *12*, 296−306.
(43) You, Y.; Niu, C.; Zhou, J.; Liu, Y.; Bai, Z.; Zhang, J.; He, F.; Zhang, N. Measurement of air exchange rates in different indoor environments using continuous CO_2 sensors. *J. Environ. Sci.* **2012**, *24*, 657−664.

https://dx.doi.org/10.1021/acs.est.0c05624
Environ. Sci. Technol. 2020, 54, 15680−15688